RESEARCH MEMORANDUM

FREE-FLIGHT INVESTIGATION AT TRANSONIC SPEEDS OF DRAG

COEFFICIENTS OF A BOATTAIL BODY OF REVOLUTION WITH

A SIMULATED TURBOJET EXHAUST ISSUING AT THE

BASE FROM CONICAL SHORT-LENGTH EJECTORS

By Ralph A. Falanga and Abraham Leiss

Langley Aeronautical Laboratory
Langley Field, Va.

NATIONAL ADVISORY COMMITTEE
FOR AERONAUTICS
WASHINGTON
December 13, 1956

NATIONAL ADVISORY COMMITTEE FOR AERONAUTICS

RESEARCH MEMORANDUM

FREE-FLIGHT INVESTIGATION AT TRANSONIC SPEEDS OF DRAG

COEFFICIENTS OF A BOATTAIL BODY OF REVOLUTION WITH

A SIMULATED TURBOJET EXHAUST ISSUING AT THE

BASE FROM CONICAL SHORT-LENGTH EJECTORS

By Ralph A. Falanga and Abraham Leiss

SUMMARY

Four $7.5°$ boattail bodies of revolution with secondary air scoops
were tested in free-flight to find the change in drag coefficient when
a simulated turbojet exhaust issued from conical short-length ejectors.
Models 1 and 2 each had single scoops and a spacing ratio l/d_p of 0.387,
whereas model 3 had two scoops and the same l/d_p as models 1 and 2.
Model 4 had a single scoop and an l/d_p of 0.097. All models tested
had the same diameter ratio d_s/d_p of 1.256. The results indicated that
the jet-on total drag coefficients were lower throughout the test Mach
number range than corresponding jet-off values of the forebody drag coef-
ficient. Furthermore, it appeared that increasing the corrected weight-
flow ratio by doubling the number of secondary scoops increased the
increment between jet-on and jet-off drag coefficients.

INTRODUCTION

The propulsive jet issuing from the base of engine nacelles or the
rearward section of fuselages can cause an appreciable reduction of the
external configuration drag (as reported in refs. 1 to 6). When the
propulsive jet was used in a short-length ejector with secondary air
flow, which was needed for cooling the engine and accessories, base and
boattail pressure drag reductions (from jet-off condition) were obtained
(as reported in refs. 7 to 11). The effect of a primary jet with sec-
ondary air flow on external configuration drag, however, has not been
fully investigated and, of the investigations conducted (refs. 7 to 11),
only reference 11 has published data covering the transonic speed range
in which present-day jet aircraft were operating. Thus, as a phase of
the current jet-effect research program at the Langley Laboratory, a

study of the effects of a jet issuing at the base from conical shroud
ejectors on the external configuration drag was made through the tran-
sonic and low supersonic speed range and is reported herein.

The investigation consisted of the free-flight testing of four
research models with conical ejector-shroud assemblies. The primary
jet issued from a sonic nozzle and simulated full-scale turbojet exhaust
parameters by use of a solid propellant rocket motor (designed according
to ref. 12). Auxiliary external inlets supplied and controlled the
amount of secondary cooling air used in the models. The variables for
the models tested were spacing ratio l/d_p and corrected weight-flow
ratio. The tests were conducted at the Langley Pilotless Aircraft
Research Station at Wallops Island, Va. Jet-off data covered a Mach
number range from 0.85 to 1.47 and jet-on data, from 0.92 to 1.47. The
Reynolds number (based on body length) varied during the jet-off phase
from 19.5×10^6 to 52×10^6 and during the jet-on phase from 25×10^6
to 46.9×10^6. The ratio of the jet static pressure to the free-stream
static pressure varied from about 3.0 to 4.2 and the corrected weight-
flow ratio varied from 0.014 to 0.044 during the jet-on phase.

SYMBOLS

A   area, sq ft

C_D' drag coefficient at secondary air-flow ratio of 0.009

C_D drag coefficient at flight secondary air-flow ratios

C_p pressure coefficient

d   diameter, ft

F_{ej} ejector gross thrust, lb

F_j primary jet thrust, lb

l distance between nozzle exit to model base, ft

M   Mach number

p   static pressure, lb/sq ft

p_t total pressure, lb/sq ft

N_{Re} Reynolds number (based on body length)

R gas constant, lb-ft/lb-$^{\circ}$R

S maximum cross-sectional area, sq ft

t time, sec

w weight flow, lb/sec

$\dfrac{w_s}{w_p}\sqrt{\dfrac{T_s}{T_p}}$ corrected weight-flow ratio of secondary air to primary jet

T temperature, $^{\circ}$R

γ ratio of specific heats

Subscripts:

b base

f forebody (excludes base of model)

p primary

s secondary

t total

w wall

∞ free stream

rms root mean square

MODELS AND APPARATUS

Models

The external fuselage of the models consisted of a parabolic nose, a cylindrical center section with a 6.5-inch diameter, and a conical boattail. The parabolic nose section, the coordinates of which are given in table I, was 26.00 inches long and the straight cylindrical section was 28.03 inches in length. The conical boattail had a 7.5° angle and was 10.97 inches long. The total length of the fuselage was 65.00 inches;

thus, the configuration had a fineness ratio of 10. Four thin 60° swept-back fins with beveled leading and trailing edges attached to the conical afterbody were used to stabilize the body in flight. Photographs of the configurations tested are shown in figure 1.

The external appearance of the test models was alike, except for the number of secondary air scoops incorporated on each model. Models 1, 2, and 4 had single scoops, whereas model 3 had two scoops which were 180° apart. Models 1 and 2 were dimensionally identical. A two-view drawing and detailed dimensions of a single-scoop model are shown in figure 2. Similar scoops were used on all the test models and a typical cross section of one scoop is shown in figure 2.

Models 1, 2, and 3 had the same spacing ratio $l/d_p = 0.387$, whereas model 4 had an l/d_p of 0.097. All models tested had the same diameter ratio $d_s/d_p = 1.256$.

Figure 3(a) shows details of the conical ejector-shroud assembly used on these models. The ejector parameters, mixing length l, spacing ratios l/d_p, and diameter ratios d_s/d_p for each model are also given in this figure. Photographs illustrating the two spacing ratios used are shown as figure 3(b). The tube and orifice (location given in fig. 3(a)) used to measure wall-exit static pressure during jet-off and jet-on flight can be seen in these photographs.

Figure 4 shows a cross section of the turbojet simulator used in the flight models. It consisted essentially of a combustion chamber, a flow-control nozzle, a plenum chamber, and a convergent sonic-exit section. The simulators utilized a modified 3.25-inch aircraft rocket combustion chamber containing a specially machined cordite SU/K solid propellant. Each turbojet simulator had a throat diameter of 1.154 inches and a sonic-exit diameter of 2.582 inches. The models had an average take-off weight of 44.30 pounds.

Model Instrumentation

A five-channel telemeter, which was carried in the nose section of each model, continuously transmitted measurements of acceleration, combustion chamber pressure, secondary-flow inlet static pressure, secondary-flow total pressure and exit-wall static pressure to ground receiving stations. The secondary-flow static-pressure orifice was located in the throat of the secondary inlet nozzle as shown in figure 2, whereas the secondary total pressure data represent an average obtained from four slotted-total pressure pickups with slots across the annular duct at approximately nacelle station 60.0. The orifice locations for the wall-exit pressure and rocket chamber pressure are shown in figures 3(a) and 4, respectively.

Data for the flight tests were obtained by use of telemeter,
CW Doppler velocimeter, tracking radar, and rawinsonde. The rawinsonde
gave a survey of the atmospheric conditions over the test altitude. The
model velocity obtained with the velocimeter was corrected for wind
velocity which was determined from rawinsonde measurements.

TEST AND ANALYSIS

Ground Tests

A preflight static firing of the turbojet simulator with the ejector-
shroud assembly of model 1 connected was made at the Langley rocket test
cell and measurements of the thrust of the system, the rocket chamber
pressure, the secondary inlet static and total pressures, and the wall-
exit pressure were recorded.

Flight Tests

The models were launched from a rail-type launcher (fig. 5) at an
angle of approximately 59°. A single 65-inch rocket motor boosted each
model to the peak Mach number. Jet-off data were obtained during the
decelerating flight after separation of the model from the booster and
after burnout of the simulator motor. Jet-on data were obtained during
the firing of the turbojet simulator. Models 1, 3, and 4 coasted to
subsonic speeds before a turbojet simulator fired, while model 2 was
fired after a short coast time to obtain a higher test Mach number with
jet on, as shown in figure 6. This produced a higher Reynolds number
for model 2 than for models 1, 3, and 4 with jet on (fig. 7), since the
altitude was lower and the free-stream static pressure greater. Simi-
larly, the jet static-pressure ratio presented in figure 8 was lower
for model 2 than for models 1, 3, and 4.

Analysis

From the data obtained in the preflight static test, a calibration
curve of the measured thrust of the system as a function of rocket chamber
pressure was made. During the preflight static test the primary jet
entrained some secondary cooling air which amounted to a corrected weight-
flow ratio of 0.009. Therefore, the measured thrust obtained from the
calibration curve included the thrust of the primary jet as well as any
effect on the measured thrust from a corrected secondary weight-flow
ratio of 0.009.

Inasmuch as the rocket chamber pressures were recorded in flight,
the thrusts of the propulsion systems for the flight models were obtained
by using the established calibration curve and an altitude correction.
These values of measured flight thrust were then used in computing jet-
on values of the drag coefficient, $\left(C_{D,on}\right)$ which have been plotted against

Mach number in figure 9. Also plotted in figure 9 are jet-off values of total drag and base drag coefficients for the models. The procedures of computing jet-on and jet-off drag coefficients and base drag coefficients were the same as those outlined in reference 1.

Reference 13 has shown that the gross thrust of a conical ejector varies with secondary air flow; that is, for a given engine thrust the gross thrust of the conical-ejector system increased as the ratio of the secondary weight flow to the primary weight flow increased. During the flight tests of the present models, the amount of secondary air inducted by the scoops varied although the primary jet remained relatively constant. Since no attempt was made during preflight static tests to evaluate the effect of the secondary weight-flow ratio on the gross thrust of the conical ejector, it was necessary to use data obtained from a comparable ejector to estimate the change in the ejector gross thrust in flight. Configuration G of reference 13 was comparable to the conical ejector used in models 1, 2, and 3; configuration G had an 8° conical shroud, an l/d_p of 0.408, and a d_s/d_p of 1.10 as compared with a 7.5° conical shroud, an $l/d_p = 0.387$, and a d_s/d_p of 1.256 for models 1, 2, and 3. Configuration G was also tested at approximately the same jet temperature and jet pressure ratio as the present models. Although the ejector geometry was slightly different, the data of reference 14 show that the effect of the differences in geometry for the jet pressure and weight-flow ratios covered was small. Thus, it was assumed that the variation of the gross thrust of the ejector with corrected secondary air-flow ratio for models 1, 2, and 3 would be the same as that of configuration G of reference 13. The slope of the curve of the ratio of the ejector gross thrust to the primary jet thrust as a function of

corrected weight-flow ratio $\dfrac{d\left(F_{ej}/F_j\right)}{d\left(w_s/w_p \sqrt{T_s/T_p}\right)}$ was determined for the

3,750° R afterburner temperature. By using this slope, the increment in the ejector gross thrust between the actual flight corrected weight-

flow ratios and that of the preflight static firing $\left(\dfrac{w_s}{w_s}\sqrt{\dfrac{T_s}{T_p}} = 0.009\right)$

was obtained. Then, this increment was added to the ejector gross thrust

obtained for $\dfrac{w_s}{w_p}\sqrt{\dfrac{T_s}{T_p}}$ of 0.009 to give the ejector gross thrust at the

flight corrected weight-flow ratios. This corrected thrust was used to compute the jet-on drag coefficients for models 1, 2, and 3 which have been plotted against Mach number in figure 10.

Model 4 had different ejector-shroud geometry than the other models (that is, $l/d_p = 0.097$) and it was assumed to perform as a zero-length ejector system. The measurements made on the secondary air-flow system of this model indicated that the secondary momentum which existed for

jet-off and jet-on flight was small and was approximately the same value. Thus, it was assumed that the gross thrust of the system was the same as the thrust of the primary jet. Therefore, the calibration curve obtained from preflight static test was modified to represent the thrust of the primary jet alone by subtracting the increase in thrust indicated by reference 13 for corrected weight-flow ratio of 0.009. This modified calibration curve was then used to determine the total thrust of model 4 and from these values the jet-on drag coefficients were computed and presented in figure 10(d).

The corrected weight-flow ratio was determined from the following ratio of the continuity equations for the secondary and primary jets:

$$\frac{w_s}{w_p}\sqrt{\frac{T_s}{T_p}} = \frac{A_s p_s M_s}{A_p p_p M_p}\sqrt{\frac{\gamma_s R_p}{\gamma_p R_s}}$$

where p_s was measured directly in flight and M_s was obtained during supersonic speeds by assuming a normal shock standing in front of the inlet and determining the free-stream total pressure entering the inlet. A zero loss was assumed from inlet entrance to inlet throat where A_s and p_s were measured. The primary weight flow was determined by using the conditions existing at the simulator sonic exit station: that is, $M_p = 1$, A_p was measured, and p_p was determined from the preflight modified calibration curve. The values used for the thermodynamic properties, γ and R, of the secondary cooling air and primary jet were as follows: $\gamma_s = 1.40$, $R_s = 53.30$, $\gamma_p = 1.25$, $R_p = 65.90$, and a primary jet temperature at approximately $4,000^\circ$ R.

Accuracy

In order to establish telemeter accuracies, statistical data have been compiled over a number of years by the Instrument Research Division of the Langley Laboratory; on the basis of these data it is believed that the maximum probable error of each measurement is about ±1 percent of the full-scale range.

The error in total jet-off drag coefficient was obtained by establishing a root-mean-square total-drag-coefficient curve for five bodies of revolution which were also the same basic bodies of revolution and were approximately the same weight as the test models (excluding the secondary scoop). A standard deviation or root-mean-square deviation from the mean-drag curve was calculated for several Mach numbers and these deviations are tabulated below. The accuracy of wall-exit pressure

coefficients was computed by using the probable instrument errors given earlier, on the basis of the foregoing, the test accuracies for jet-off conditions are within the values tabulated below:

Mach number	$C_{p,w}$	$\Delta C_{D,t,rms}$
0.95	±0.015	±0.0103
1.10	±.005	±.0058
1.30	±.005	±.0058

The velocity measured by the CW Doppler velocimeter is known to have an error of less than 1 percent. Since Mach number is determined from velocity, the above quoted errors also apply to Mach number.

The degree of accuracy obtained for the computed jet-on drag coefficients was based mainly on the accuracy with which the thrusts of the rocket motor could be calculated since the absolute values of the thrust were about four to ten times greater than those of the drag for all models tested. It was conceivable that a maximum probable error of ±10 pounds of thrust could have been inherent in the technique used for obtaining flight thrust values (because of the quoted probable error of the static thrust stand employed in the preflight testing phase of the simulator). This error corresponds to an error in jet-on drag coefficients of ±0.044 at $M = 0.95$, ±0.033 at $M = 1.10$, and ±0.025 at $M = 1.30$.

RESULTS AND DISCUSSION

Drag

The variation of jet-off and jet-on total drag coefficients and jet-off base drag coefficients with free-stream Mach number for the present models is presented in figure 9. These total drag coefficients (jet off and jet on) were obtained by using the measured flight data and preflight calibration curve as outlined in the analysis section. The jet-off base drag coefficients for the models tested have the same general trends, that is, negative or thrusting values in the transonic region and, except for model 2, have slightly positive values in the supersonic region. The jet-off base drag coefficients for model 2 remain slightly negative in the supersonic region, but the difference which exists between this model and the others is negligible, that is, the difference lies within the accuracy of the data. Models 1, 2, and 4, the single-scoop models, have about the same magnitude of jet-off total drag coefficients throughout the test Mach number range whereas model 3, the double-scoop model, has

about a 20 percent higher drag coefficient in the supersonic region.
The jet-on total drag coefficients, $C_{D,on}^j$ for all models tested were
lower than the jet-off values throughout the test Mach number range,
model 3 having the largest reduction.

The jet-on values of drag coefficients presented in figure 10 have
been altered from those presented in figure 9 by including the estimated
effect on the measured flight values of thrust due to differences in
secondary rate flows in the conical ejector system from that used in the
preflight static test. The procedure, by which the gross thrust of the
conical ejector systems for models 1, 2, 3, and 4 were obtained, has
been outlined previously in the analysis section.

Figure 10 shows the variation of jet-on total drag coefficient and
the jet-off forebody drag coefficients (total drag minus base drag) as
a function of free-stream Mach number. This plot shows that the magnitude
of jet-on total drag coefficients is lower throughout the test Mach number
range than the jet-off forebody values for all models tested. The dif-
ferences which exist between the jet-off forebody drag coefficients and
jet-on total-drag coefficients are an indication of the amount the jet-off
boattail and fin drag coefficients have been reduced by operation of the
jet, the largest reduction appearing in model 3 (fig. 10(c)) which inci-
dently had the maximum amount of secondary cooling air mixing with the
primary jet.

Figure 11 summarizes the jet-off forebody drag $C_{D,f}$ and jet-on
total drag coefficients for models with no scoop (model 3 of ref. 1),
single scoop, and double scoop. The jet-off forebody-drag-coefficient
curve for the single-scoop model represents a mean curve derived from
models 1, 2, and 4. The addition of scoops to take in secondary air flow
increased the jet-off forebody drag coefficients above those for the no-
scoop model, and the magnitude of the increase was almost twice as great
for the double-scoop model as it was for the single-scoop models. There
appears to be an effect of supersonic Mach number on the magnitude of the
increase; that is, as the Mach number increases above 1.2, the change in
forebody drag coefficient between the no-scoop model and models with
scoops tends to increase. Figure 11 shows that, when the propulsive jets
were operated, the drag coefficients were reduced from the jet-off values.
For all models tested, the jet-on total drag coefficients were somewhat
greater than those of the no-scoop model, but the magnitude of drag reduc-
tion between the jet-on and jet-off conditions for all models represented
in this plot were of the same order of magnitude. Also, within the accu-
racy of the test results, increasing the amount of secondary air flow by
doubling the number of scoops tended to increase the increment in drag
coefficient between jet-on and jet-off flight. Although decreasing the
ejector-spacing ratio l/d_p (model 4) tended to decrease the increment
between the jet-on and jet-off drag coefficients.

The corrected weight-flow ratio $\frac{w_s}{w_p}\sqrt{\frac{T_s}{T_p}}$ varied from approximately 0.014 to 0.020 for model 1, 0.019 to 0.028 for model 2, 0.025 to 0.044 for model 3, and 0.014 to 0.021 for model 4. (See fig. 13.) This variable $\frac{w_s}{w_p}\sqrt{\frac{T_s}{T_p}}$ appears to have some effect on the magnitude of drag reduction obtained for all models tested, but it is difficult here to separate the effects of jet static-pressure ratio p_p/p_∞ and $\frac{w_s}{w_p}\sqrt{\frac{T_s}{T_p}}$ on the magnitude of the reduction obtained. Some indication of the effect of increasing $\frac{w_s}{w_p}\sqrt{\frac{T_s}{T_p}}$ on the magnitude of drag reduction can be observed from the larger increment in drag obtained for model 3 over the others (figs. 10 and 11). In general then, by increasing $\frac{w_s}{w_p}\sqrt{\frac{T_s}{T_p}}$ for the models tested, there appears to be a tendency towards further reduction in jet-on total drag coefficients from jet-off values.

Ejector-Shroud Characteristics

Figure 12 presents the variation of jet-off and jet-on wall-exit pressure coefficient with free-stream Mach number for models 1, 2, 3, and 4. It has been assumed that the jet-off wall-exit pressures are representative of the magnitude of the pressure which existed across the base and, as a result, they have been used to compute the base drag coefficients which were presented in figure 9.

The operation of the primary jet increased the wall-exit pressure coefficient $C_{p,w}$ for all models tested. Within the limits of these data, models 2 and 3 appear to fair into a continuous curve that falls well below that of model 1. Inasmuch as the ejector geometry for models 1, 2, and 3 was the same and the total pressure of the primary jet $p_{t,p}$ was relatively constant for these models, it appears that one of the reasons that the value of $C_{p,w}$ of models 2 and 3 falls below that of model 1 can be attributed to the differences in total pressure of the secondary air flow $p_{t,s}$ between that of model 1 and that of models 2 and 3. Figure 13, a plot of the variation of $p_w/p_{t,p}$ with $p_{t,s}/p_{t,p}$, shows that $p_{t,s}$ for models 2 and 3 is approximately the same over a portion of the range covered and is considerably greater than the $p_{t,s}$ values of model 1. Although there were not enough measurements made in these tests to determine the reason that $p_{t,s}$ affects $C_{p,w}$, it is felt that the secondary air flow tends to act like a cushion between the

conical shroud wall and the primary jet. Thus, as $p_{t,s}$ increases, the cushioning effect increases and causes $C_{p,w}$ to decrease.

The jet-on value of $C_{p,w}$ for model 4 appears to remain relatively constant throughout the test Mach number range. When the jet-on value of $C_{p,w}$ of model 4 is compared with the values for the other test models, it shows the least amount of influence of the primary jet on $C_{p,w}$. The location of the wall-exit pressure orifice for model 4 was approximately in the same plane as the exit of the primary nozzle whereas, for the other models it was about 0.29 jet diameters downstream. Thus, the primary jet had much less chance of influencing the value of $C_{p,w}$ for model 4 than it had for the other models.

In figure 13, the variation of the ratio of wall-exit pressure to the total pressure of the primary jet $p_w/p_{t,p}$ with the total-pressure ratio of the secondary to primary jet $p_{t,s}/p_{t,p}$ has been plotted for the present models. The data for the ejectors of the same geometry (models 1, 2, and 3) were plotted and formed a continuous curve which is within the accuracy of the data. The variation, which existed in this curve for the limited range of $p_{t,s}/p_{t,p}$ covered, was felt to be due mainly to the effect of $p_{t,s}$ on p_w. As $p_{t,s}$ was increased, p_w decreased for relatively constant values of $p_{t,p}$. The $p_w/p_{t,p}$ data for model 4 were approximately 40 percent lower than the data for the higher spacing ratios. It appears that the value of $p_w/p_{t,p}$ for model 4 was insensitive to any increase in $p_{t,s}/p_{t,p}$ for the limited range covered.

In order to give some indication of the pumping performance for the ejector-shroud assemblies used in the present models (fig. 14), the variation of the total-pressure ratio of the secondary jet to the primary jet with corrected weight-flow ratio has been prepared. Figure 14(a) is a comparison of the pumping performances obtained for models 1, 2, and 3 $\left(l/d_p = 0.387\right)$ with results obtained from reference 13 (configuration G) and reference 14 (configuration with l/d_p of 0.39 and d_s/d_p of 1.21). Although the spacing ratios and diameter ratios from these references were not exactly equal to values of the present models, nonetheless, it was felt that such a comparison would at least indicate that the ejector-pumping-performance data obtained for the present models were in general agreement. The solid curve presented in this plot was obtained from a cross plot of the data presented in reference 14 which had a temperature ratio of 1.0 (cold jets). Data of reference 13 presented in this plot show the variation of afterburning and nonafterburning temperatures on

the pumping performance of configuration G. Also plotted in figure 14(a) are some pumping-performance data obtained from the preflight static test (dashed circular symbols). Model 4 could not be included in the comparison with the other models because of the pronounced difference in spacing ratio $(l/d_p = 0.097)$; thus, the pumping-performance data of model 4 have been presented in figure 14(b).

CONCLUSIONS

Four 7.5° boattail bodies of revolution with secondary air scoops, a diameter ratio of 1.256, and spacing ratios of 0.387 and 0.097 were tested in free flight with a turbojet simulator to determine the effect of a primary jet with secondary air flow on the configuration drag in the transonic and supersonic speed ranges. Jet-off data covered a Mach number range from 0.85 to 1.47 and jet-on data from 0.92 to 1.47. The Reynolds number (based on body length) for the jet-off data varied from 19.5×10^6 to 52×10^6 and for the jet-on data, from 25×10^6 to 46.9×10^6. The jet to free-stream static-pressure ratio varied from approximately 3.0 to 4.2. The data obtained for the models indicated the following conclusions:

1. The addition of scoops to induct secondary air flow increased the jet-off forebody drag coefficients above those for the configuration with no secondary scoops. The magnitude of the increase was almost twice as great for the double-scoop model as it was for the single-scoop models.

2. When the propulsive jets were operated, the drag coefficients were reduced from the values obtained with the jet off. For all models tested the jet-on total drag coefficients were somewhat greater than those obtained for the no-scoop model, but the drag reduction between jet-on and jet-off conditions for all models represented was of the same order of magnitude.

3. Within the accuracy of the test results, increasing the amount of secondary air flow by doubling the number of scoops tends to increase the increment in drag coefficient between jet-on and jet-off flight

conditions. Decreasing the ejector-spacing ratio tended to decrease
the increment between jet-on and jet-off drag coefficients.

Langley Aeronautical Laboratory,
    National Advisory Committee for Aeronautics,
        Langley Field, Va., August 10, 1956.

REFERENCES

1. Falanga, Ralph A.: A Free-Flight Investigation of the Effects of Simulated Sonic Turbojet Exhaust on the Drag of a Boattail Body With Various Jet Sizes From Mach Number 0.87 to 1.50. NACA RM L55F09a, 1955.

2. Henry, Beverly Z., Jr., and Cahn, Maurice S.: Preliminary Results of an Investigation at Transonic Speeds To Determine the Effects of a Heated Propulsive Jet on the Drag Characteristics of a Related Series of Afterbodies. NACA RM L55A24a, 1955.

3. Cortright, Edgar M., Jr., and Kochendorfer, Fred D.: Jet Effects on Flow Over Afterbodies in Supersonic Stream. NACA RM E53H25, 1953.

4. Englert, Gerald W., Vargo, Donald J., and Cubbison, Robert W.: Effect of Jet-Nozzle-Expansion Ratio on Drag of Parabolic Afterbodies. NACA RM E54B12, 1954.

5. Love, Eugene S.: Aerodynamic Investigation of a Parabolic Body of Revolution at Mach Number of 1.92 and Some Effects of an Annular Jet Exhausting From the Base. NACA RM L9K09, 1950.

6. Falanga, Ralph A.: A Free-Flight Investigation of the Effects of a Sonic Jet on the Total-Drag and Base-Pressure Coefficients of a Boattail Body of Revolution From Mach Number 0.83 to 1.70. NACA RM L55L21, 1956.

7. Gorton, Gerald C.: Pumping and Drag Characteristics of an Aircraft Ejector at Subsonic and Supersonic Speeds. NACA RM E54D06, 1954.

8. O'Donnell, Robert M., and McDearmon, Russell W.: Experimental Investigation of Effects of Primary Jet Flow and Secondary Flow Through a Zero-Length Ejector on Base and Boattail Pressures of a Body of Revolution at Free-Stream Mach Numbers of 1.62, 1.93, and 2.41. NACA RM L54I22, 1954.

9. Love, Eugene S., and O'Donnell, Robert M.: Investigation at Supersonic Speeds of External-Drag Effects and Pumping Characteristics of a Short Ejector. NACA RM L55D28, 1955.

10. Cortright, Edgar M., Jr., and Schroeder, Albert H.: Preliminary Investigation of Effectiveness of Base Bleed in Reducing Drag of Blunt-Base Bodies in Supersonic Stream. NACA RM E51A26, 1951.

11. Pel, C., and Rustemeyer, A.: Investigation of Turbojet Exhaust-Interference Drag. Rep. R-0801-12, United Aircraft Corp. Res. Dept., Nov. 1955.

12. De Moraes, Carlos A., Hagginbothom, William K., Jr., and Falanga, Ralph A.: Design and Evaluation of a Turbojet Exhaust Simulator, Utilizing a Solid-Propellant Rocket Motor, for Use in Free-Flight Aerodynamic Research Models. NACA RM L54I15, 1954.

13. Greathouse, W. K.: Preliminary Investigation of Pumping and Thrust Characteristics of Full-Size Cooling-Air Ejectors at Several Exhaust-Gas Temperatures. NACA RM E54A18, 1954.

14. Greathouse, W. K., and Hollister, D. P.: Preliminary Air-Flow and Thrust Calibrations of Several Conical Cooling-Air Ejectors With a Primary to Secondary Temperature Ratio of 1.0. I - Diameter Ratios of 1.21 and 1.10. NACA RM E52E21, 1952.

TABLE I.- COORDINATES OF PARABOLIC NOSE

[Station measured from fuselage nose]

Station, in.	Ordinate, in.
0	0
1	.245
2	.481
4	.923
6	1.327
10	2.019
14	2.558
18	2.942
22	3.173
26	3.250
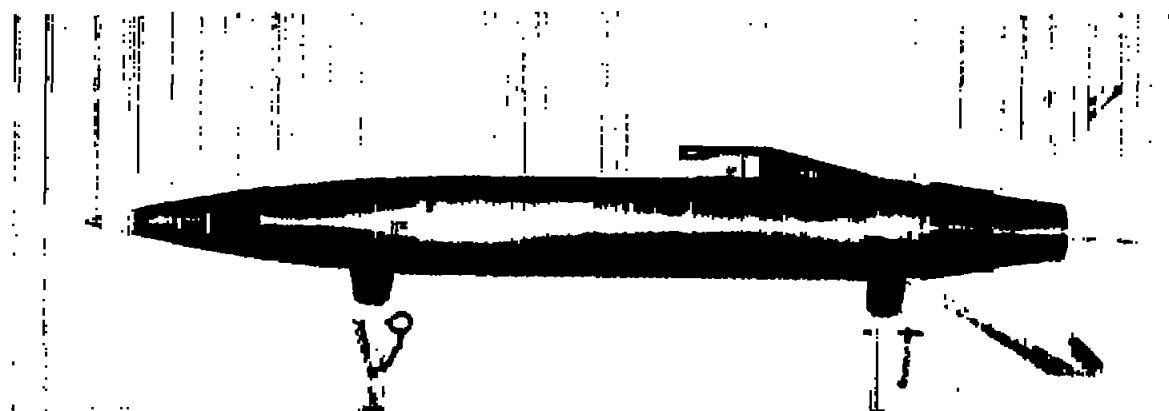
(a) Models 1, 2, and 4 (single-scoop models).   L-90310
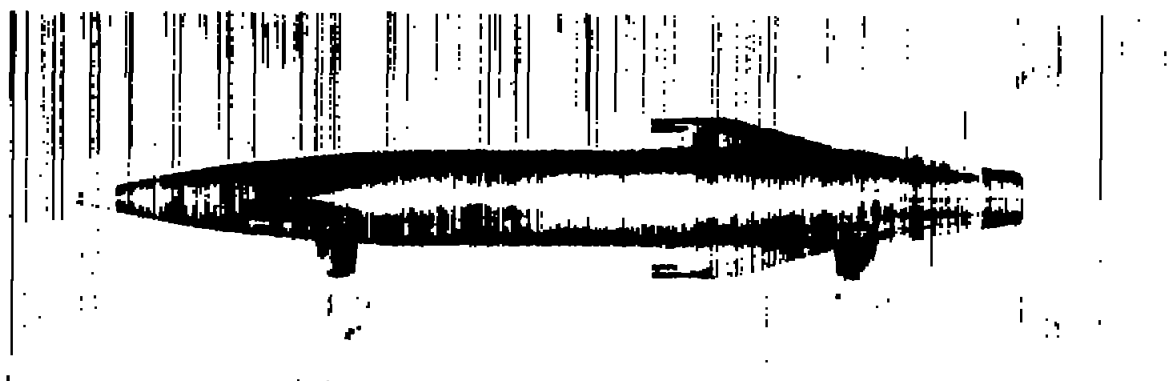
(b) Model 3 (double-scoop model).   L-90194

Figure 1.- Photographs of external configurations for the models tested.

See detail A

4.42

60°

15°

9.10

L00

6.50 Max. dia.

7.50°

3.44

2.582 Motor exit

A

A

24.00

15.182

12.625

10.97

65.00

Throat

1.28

1.22

.675

.737

.565

3.00

6.125

3.00

0.188

0.875

10° (L.E. & T.E.)

Typical fin section A-A

Mahogany
wood fairing

B

2

B

Typical scoop wood fairing section B-B

1.15

Secondary static-pressure tube

Detail A
Secondary flow scoop
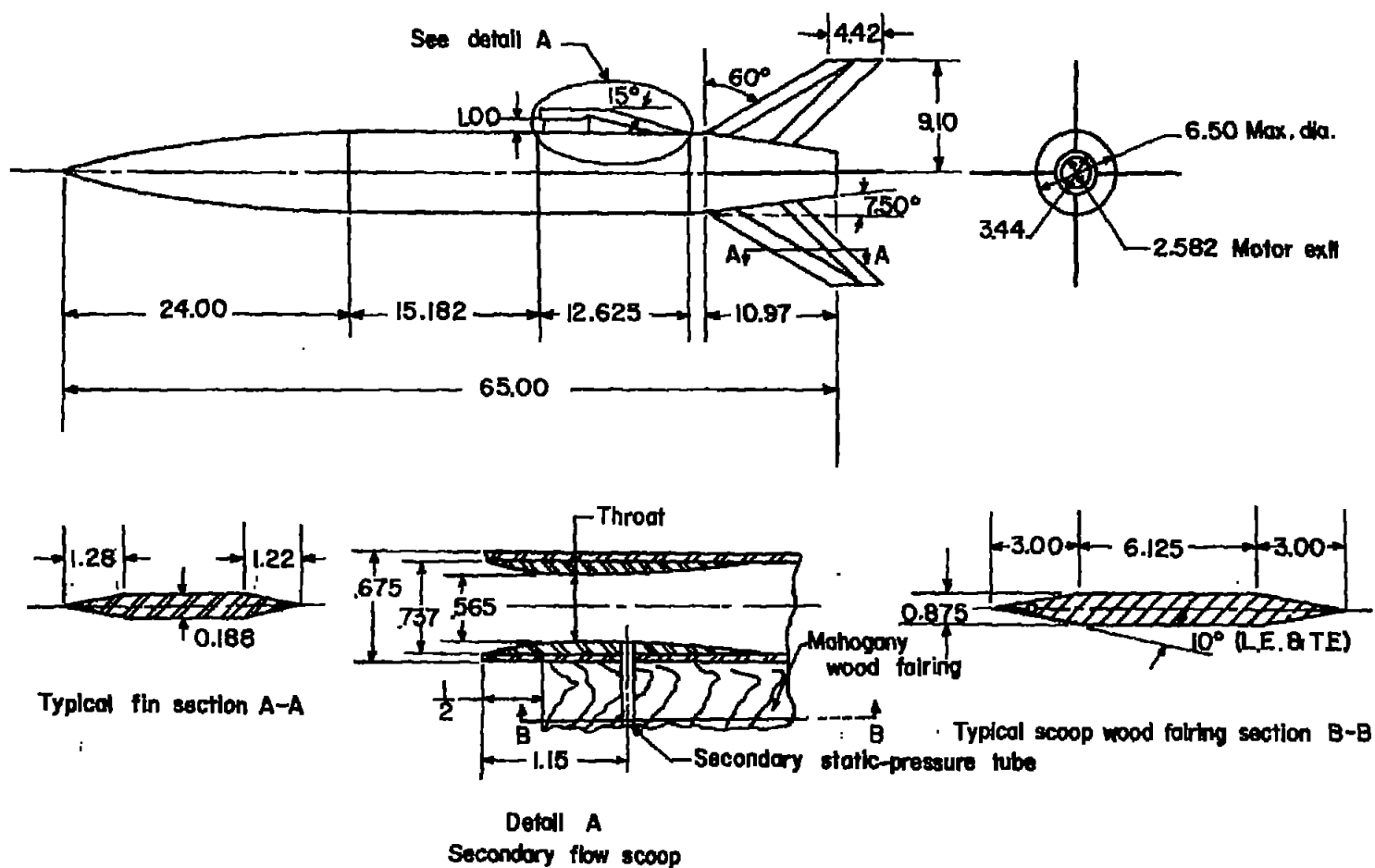
Figure 2.- Details and dimensions for a typical test model. All dimen-
sions are in inches.
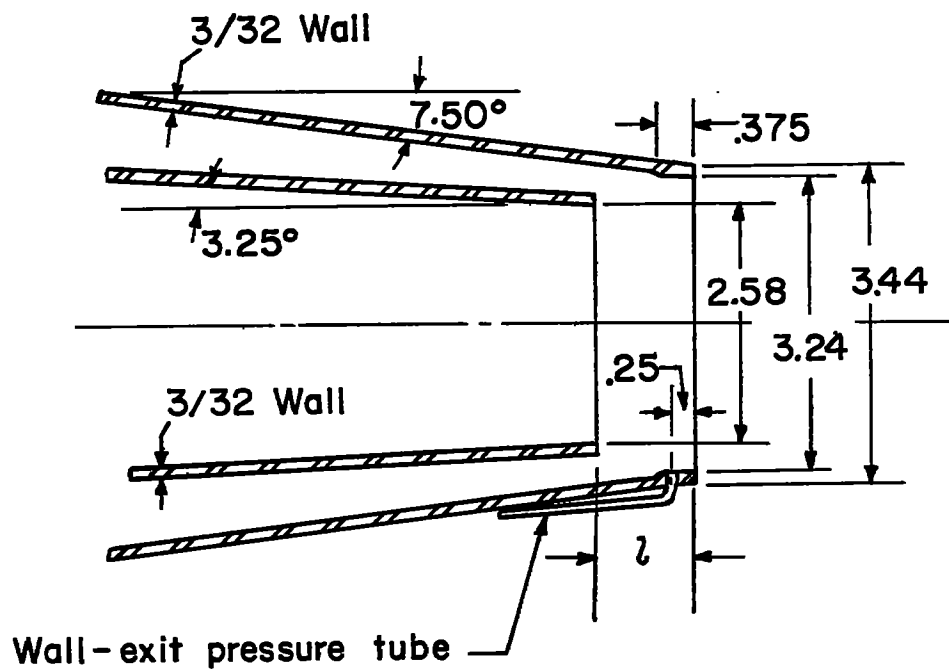
Model	Mixing length, l	Spacing ratio, l/d_p	Diameter ratio, d_s/d_p
1	1.00	0.387	1.256
2	1.00	.387	1.256
3	1.00	.387	1.256
4	.25	.097	1.256

(a) Detail and dimensions of the conical ejector-shroud assembly used. All dimensions are in inches.

Figure 3.- Some ejector-shroud assembly characteristics.

Wall-exit pressure tube

Wall-exit pressure tube
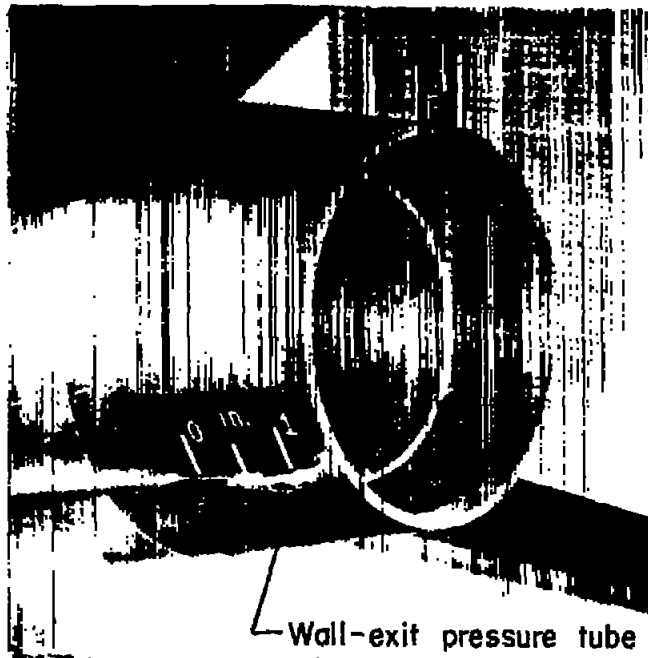
Models 1, 2, and 3 (l/d_p = 0.387)

Model 4 (l/d_p = 0.097)

L-95776

(b) Photographs of ejector-shroud assemblies used.

Figure 3.- Concluded.

Combustion chamber static-
pressure tube

Igniter

3.25

A

10

2.582
Exit dia.

Rocket case

.070 wall

1.154 Throat diameter

Head cap

Propellant

Nozzle

Grid

Plenum chamber
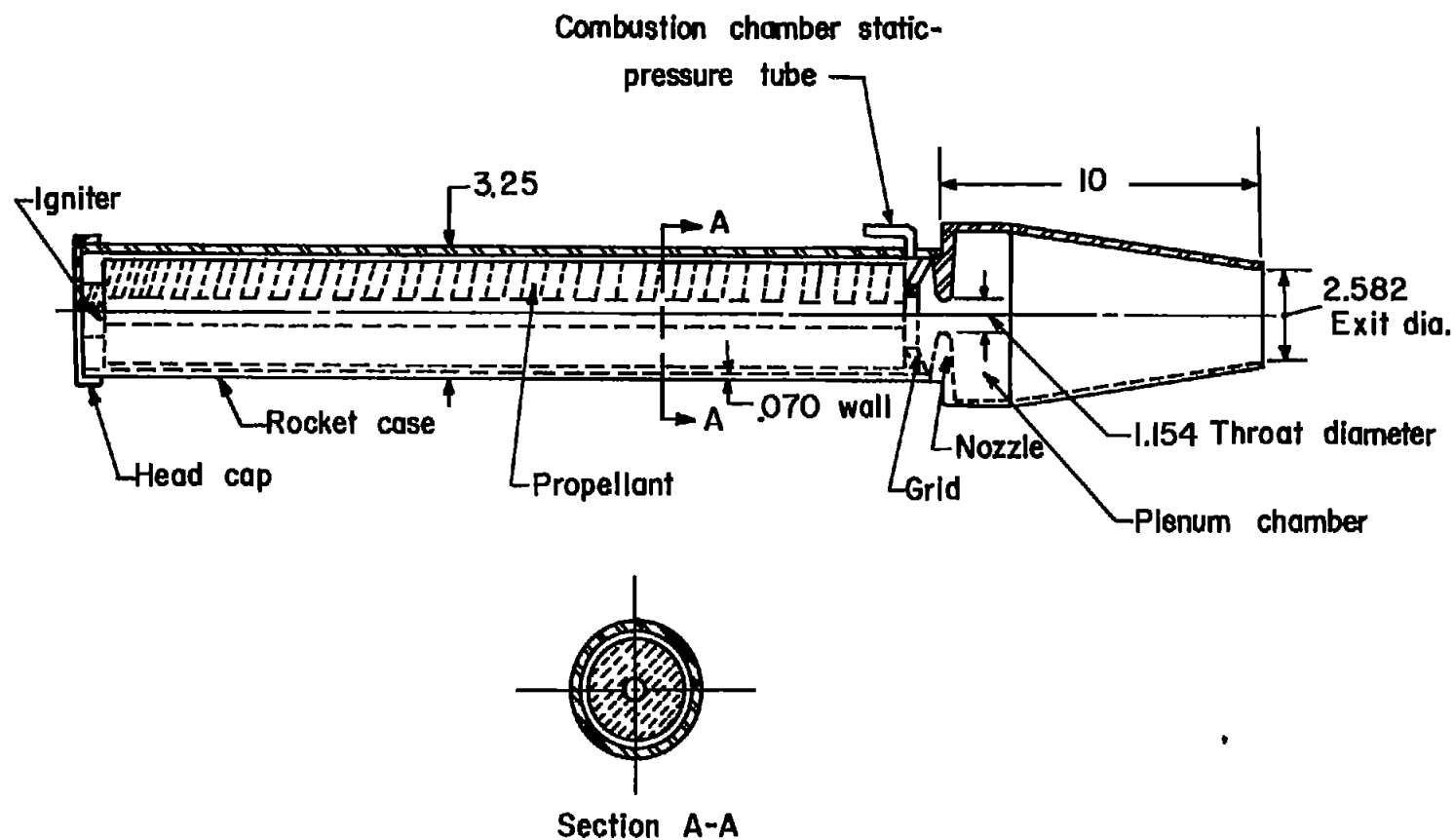
Section A-A

Figure 4.- Cross section of typical turbojet simulator. All dimensions
are in inches.
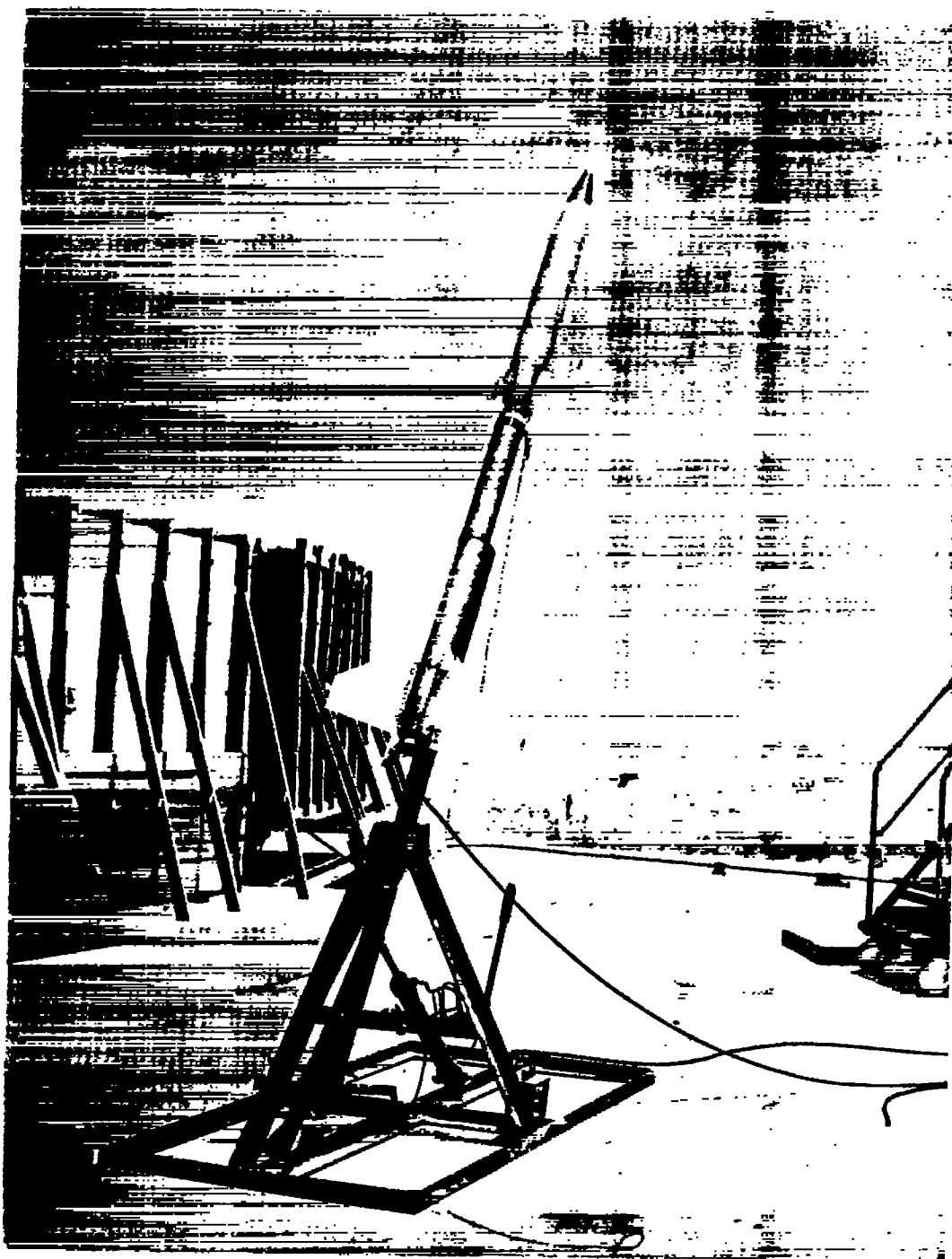
L-90105.1

Figure 5.- Photograph of model and booster on launcher.
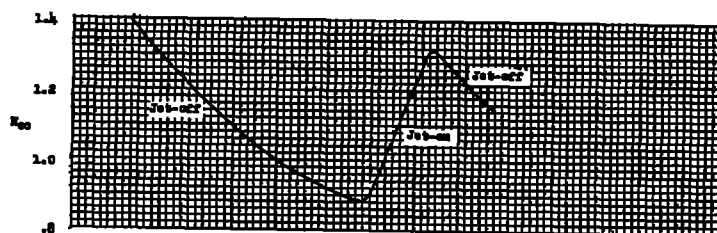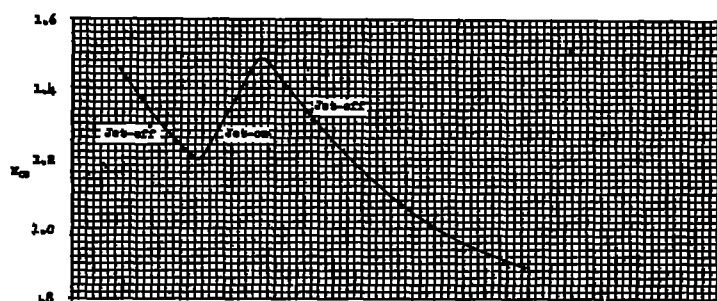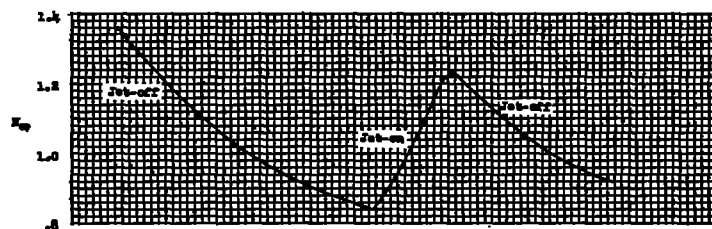
(a) Model 1.
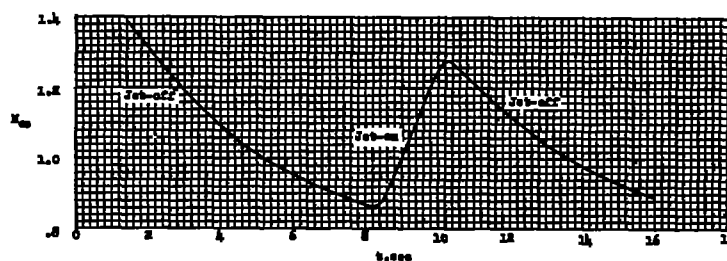
(b) Model 2.

(c) Model 3.

(d) Model 4.

Figure 6.- Variation of free-stream Mach number with time for the models tested.
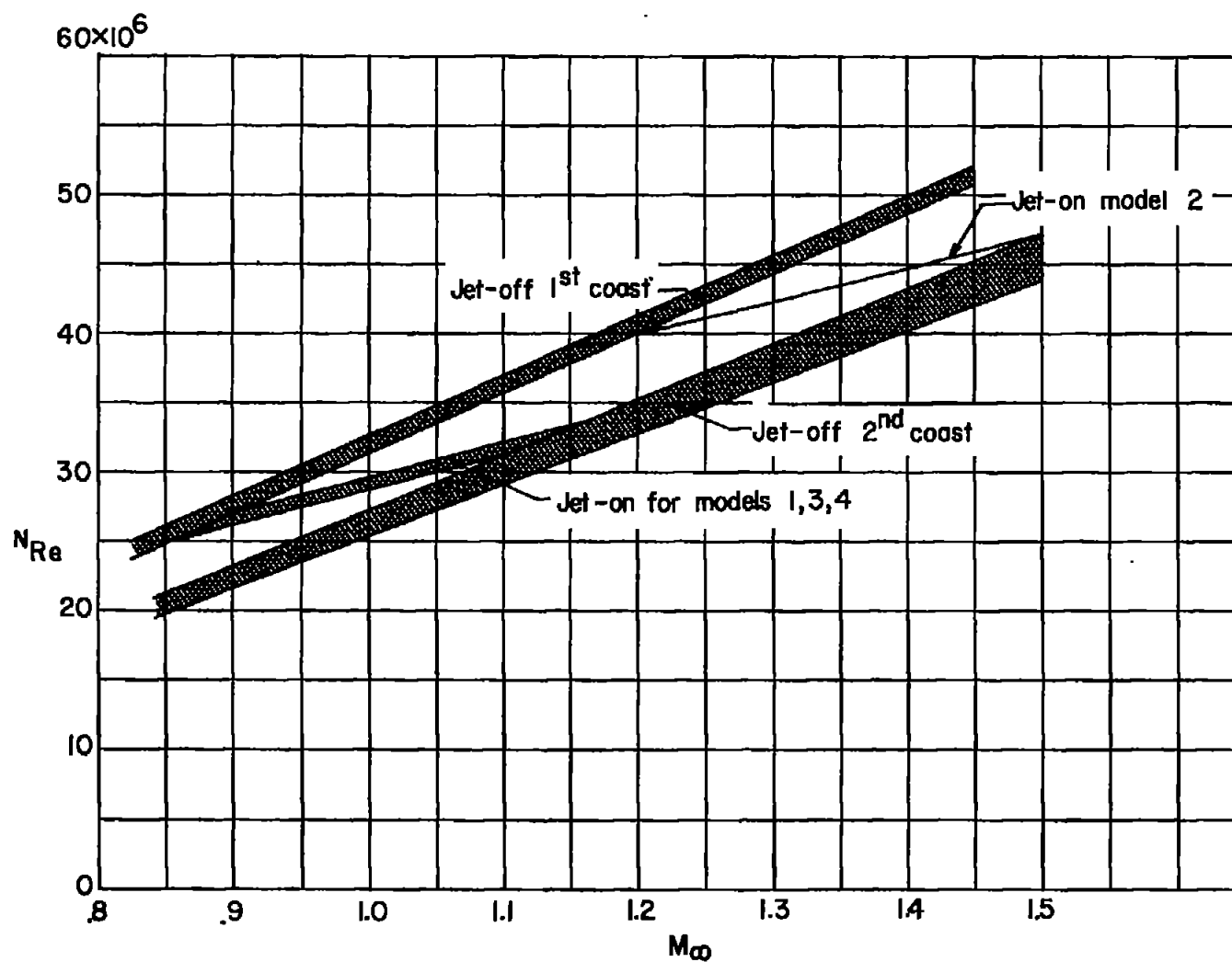
Figure 7.- Variation of Reynolds number with Mach number for all models tested. Reynolds number is based on body length.
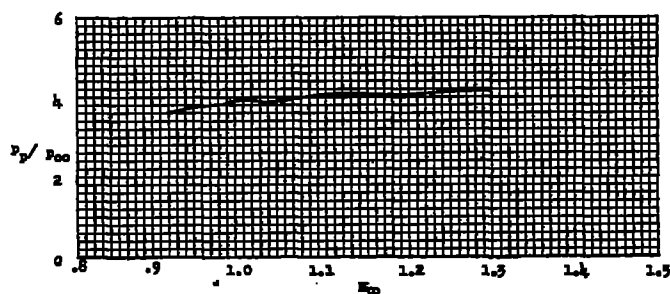
(a) Model 1.
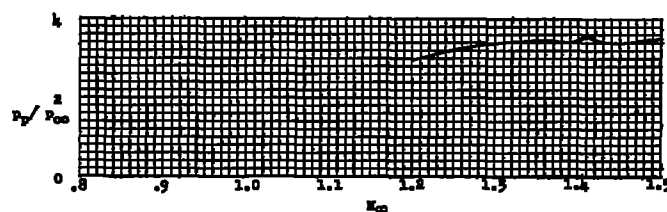
(b) Model 2.
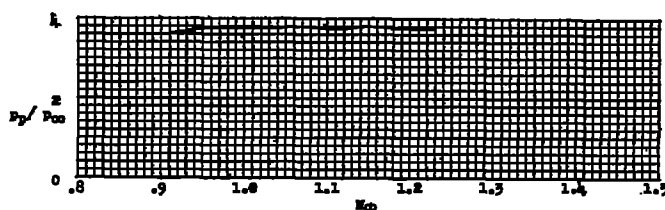
(c) Model 3.
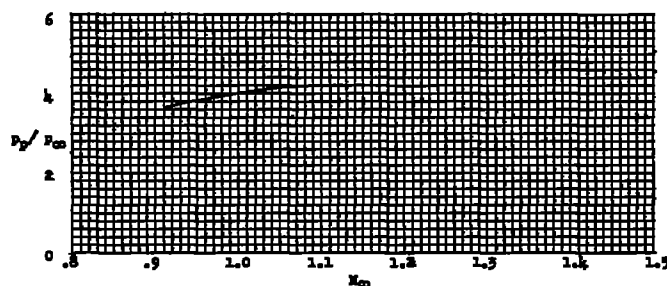
(d) Model 4.

Figure 8.- Variation of jet static-pressure ratio with free-stream Mach number for the models tested.
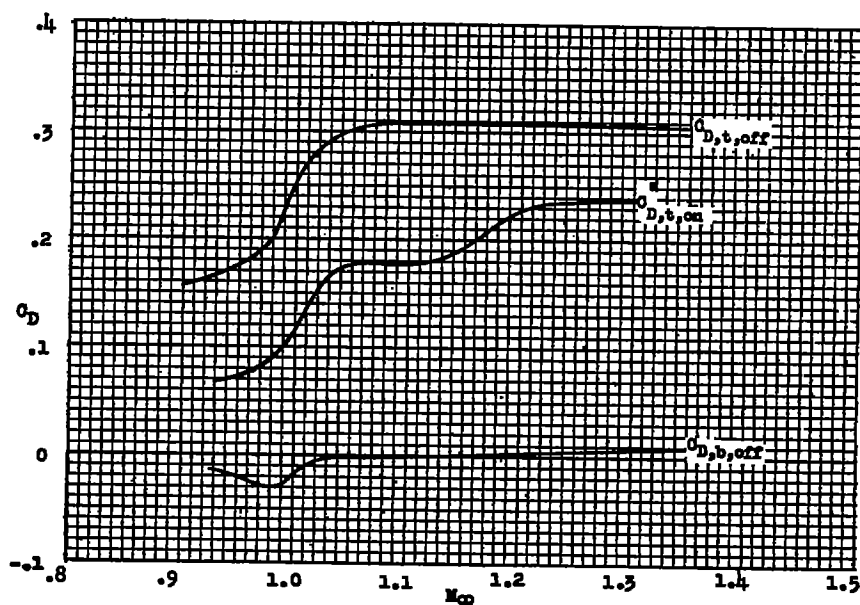
(a) Model 1.
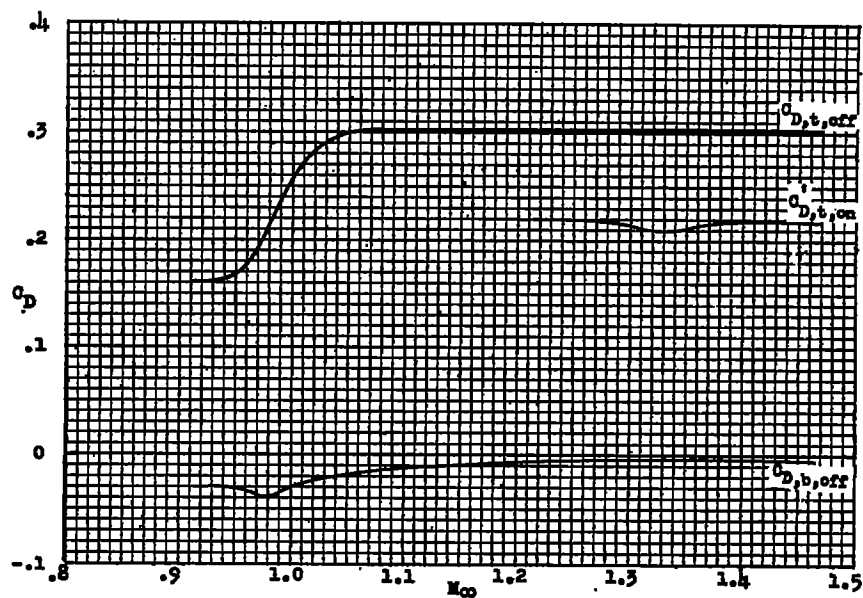
(b) Model 2.

Figure 9.- Variation of jet-off and jet-on total-drag coefficient and jet-off base drag coefficient with free-stream Mach number.
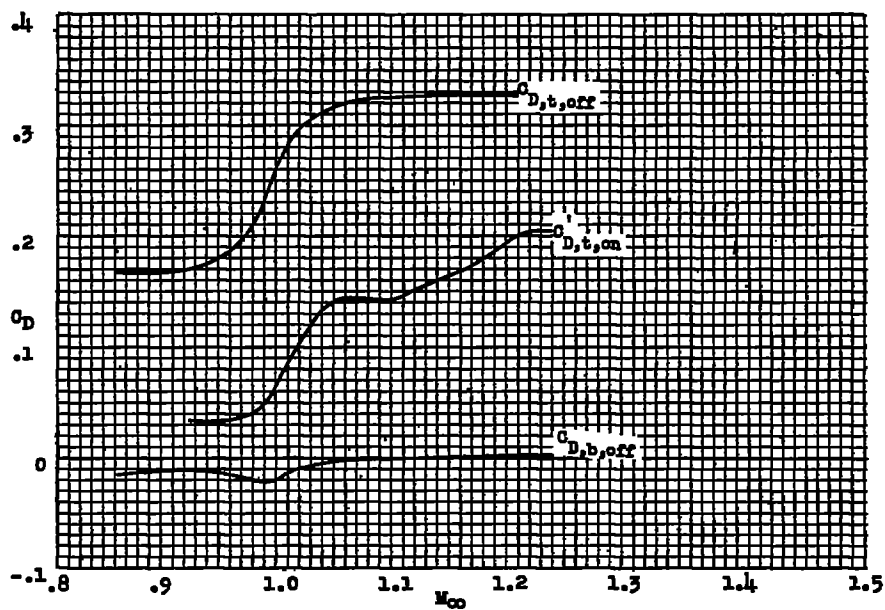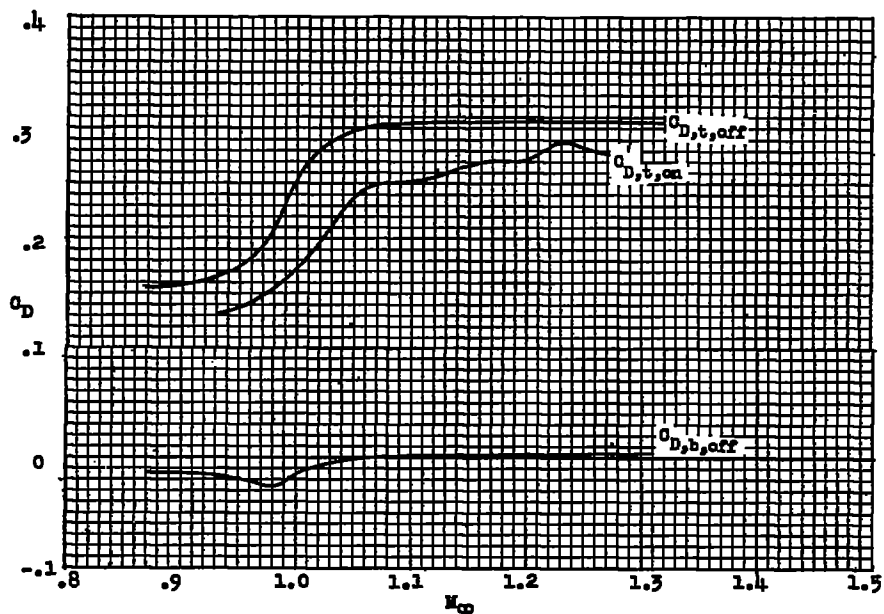
(c) Model 3.

(d) Model 4.

Figure 9.- Concluded.
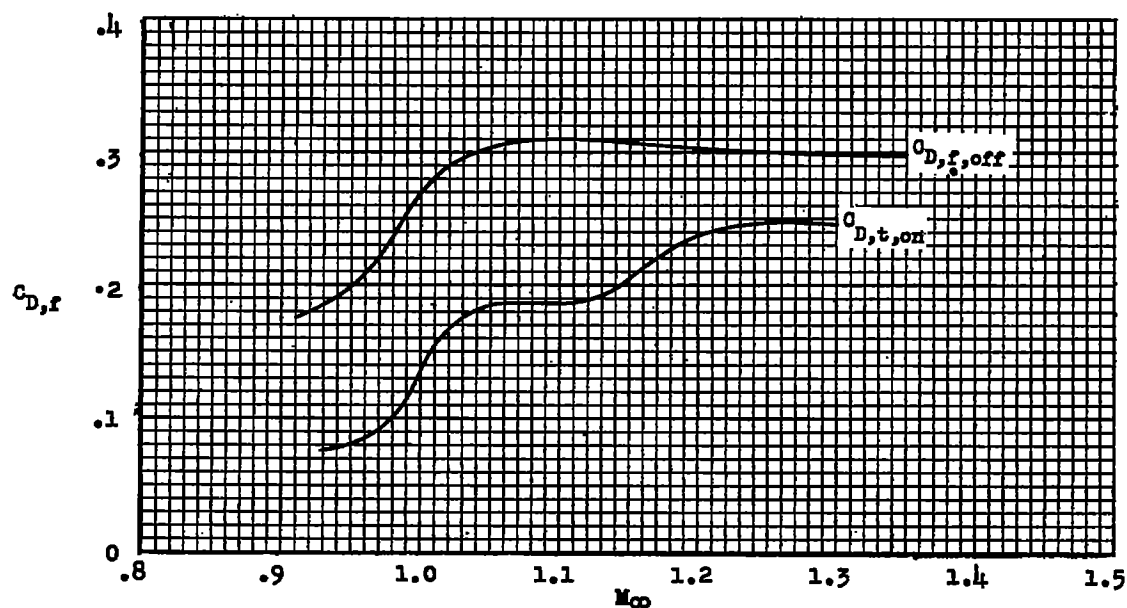
(a) Model 1.
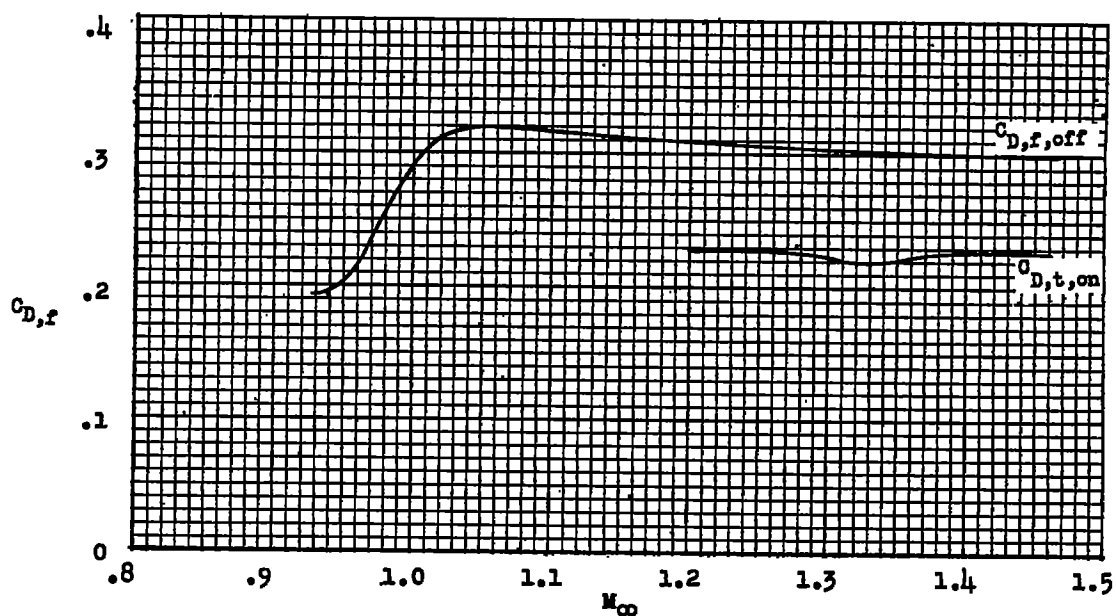
(b) Model 2.

Figure 10.- Variation of jet-off and jet-on forebody drag coefficient
(total drag minus base drag) with free-stream Mach number.
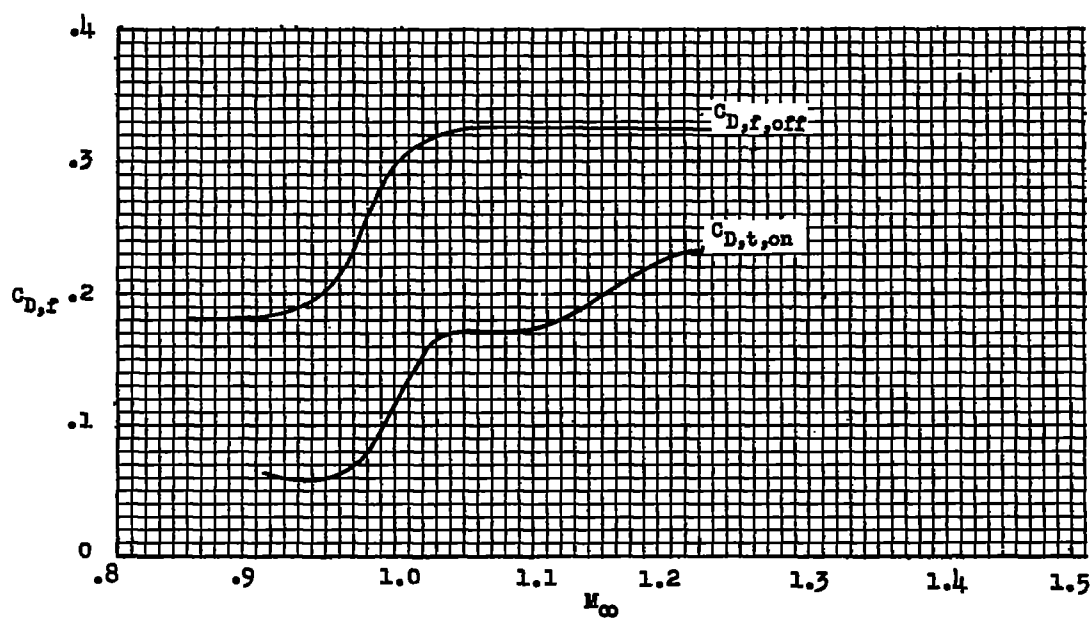
(c) Model 3.
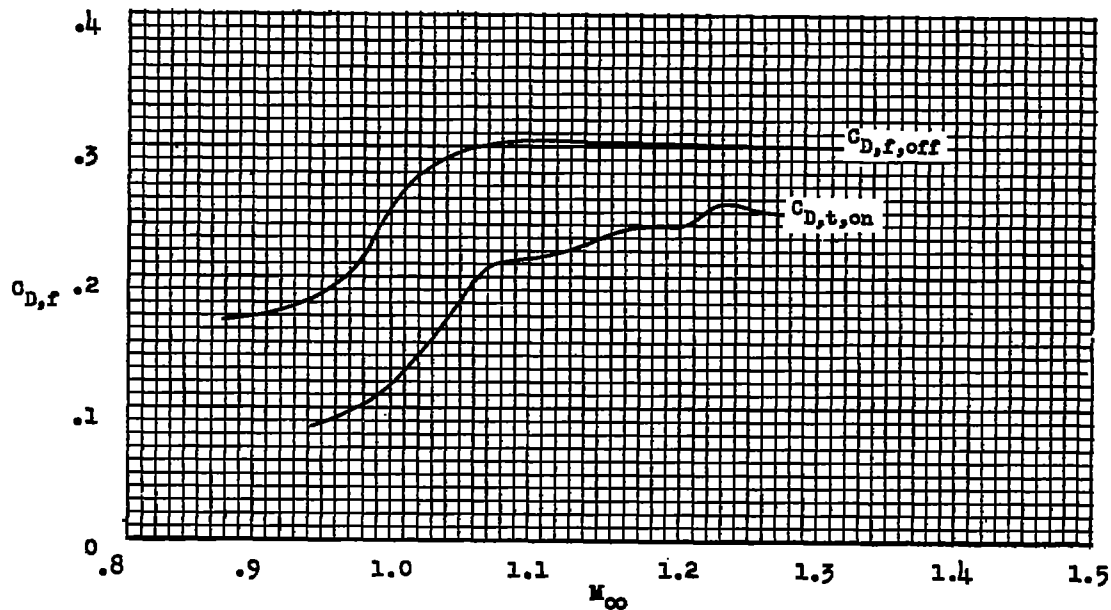
(d) Model 4.

Figure 10.- Concluded.
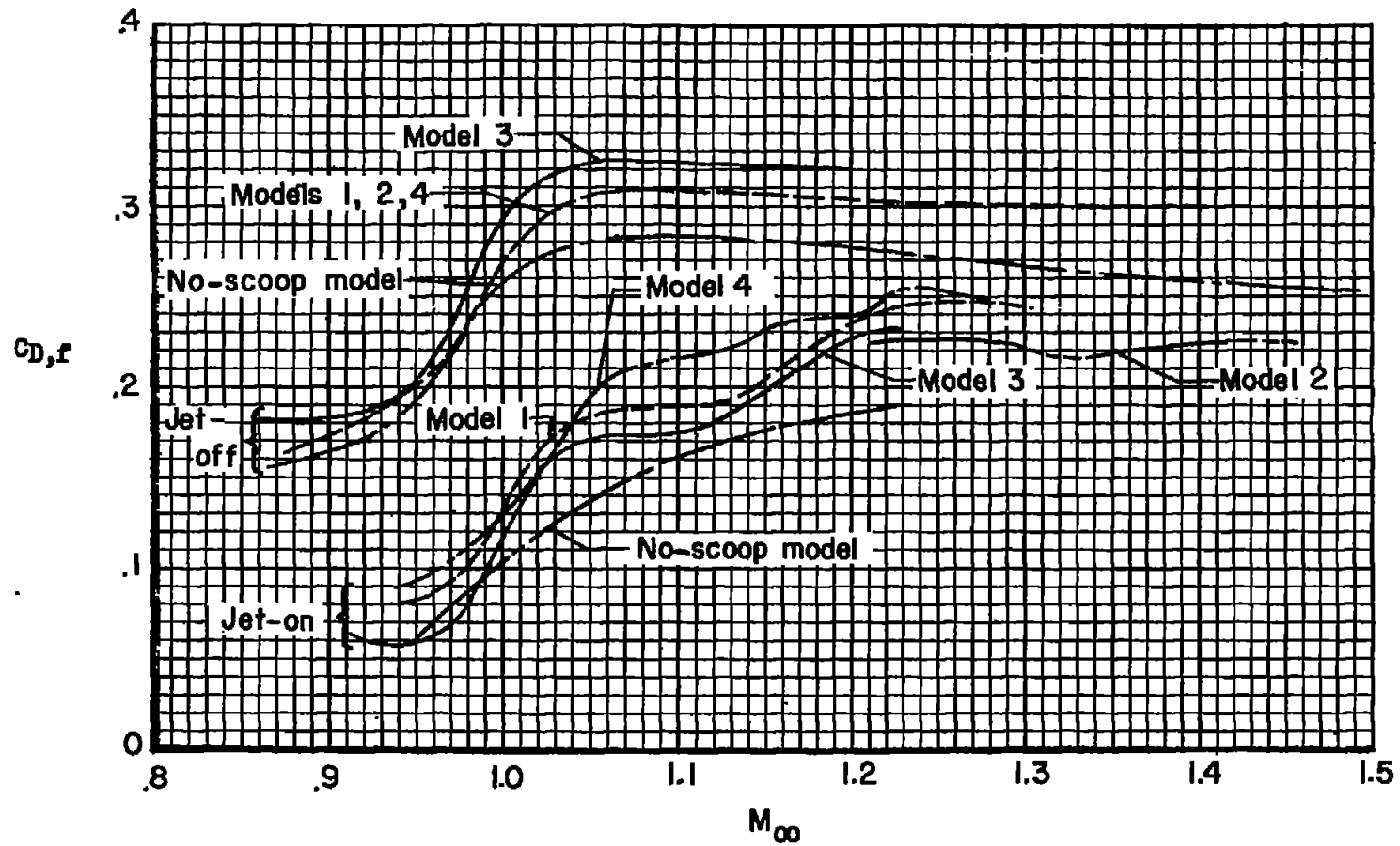
Figure 11.- Summary of the variation of jet-off forebody and jet-on drag
    coefficients with free-stream Mach number for models having no scoops,
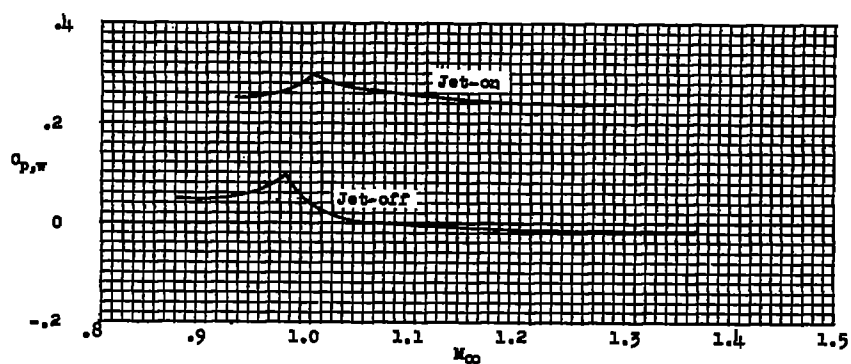   single scoops, and double scoops.
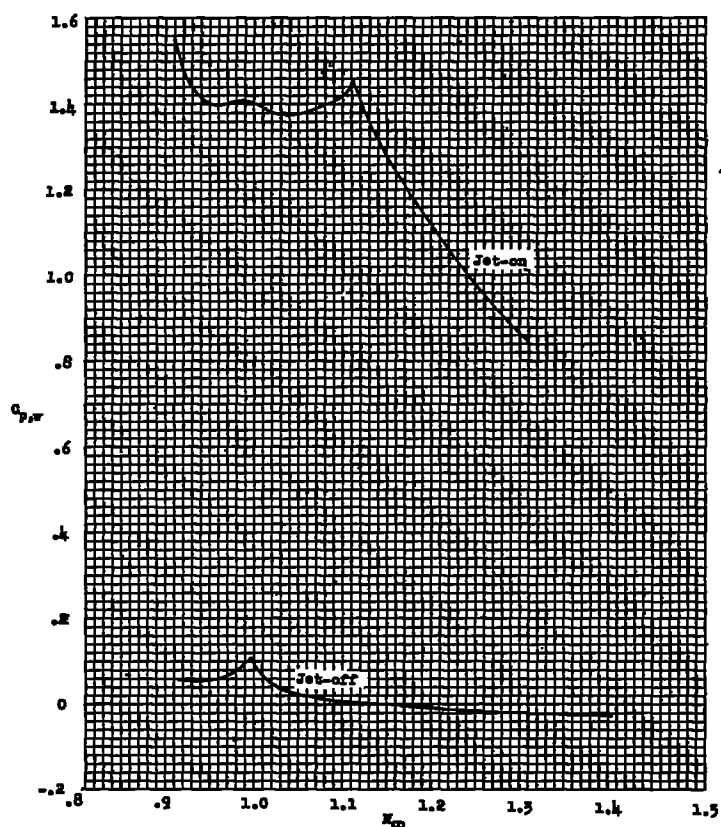
(a) Model 1.
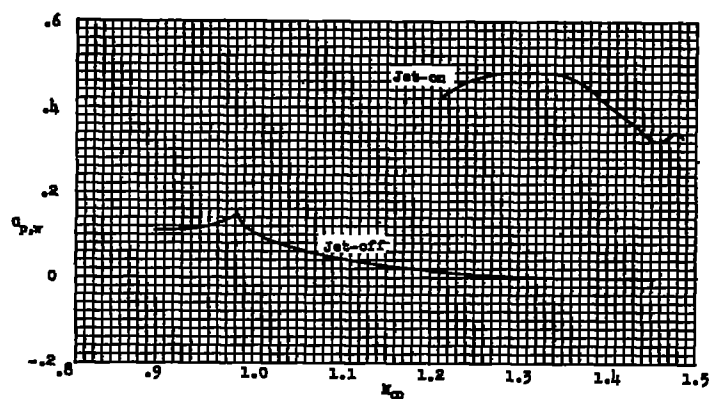
(b) Model 2.

Figure 12.- Variation of wall-exit-static pressure coefficient with free-stream Mach number.
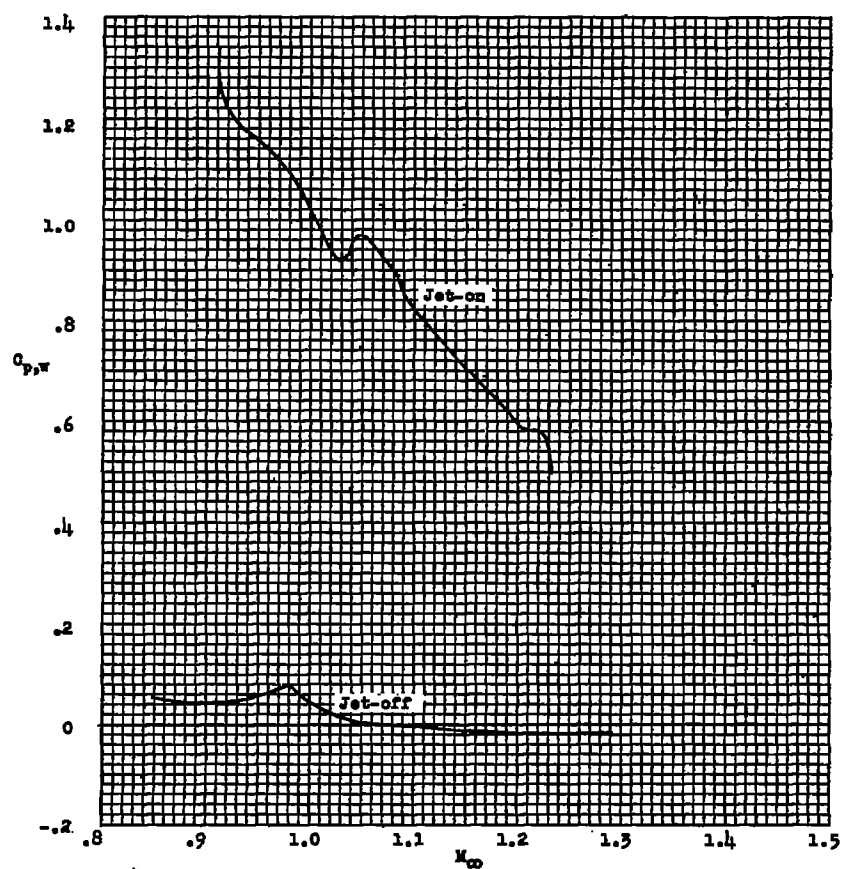
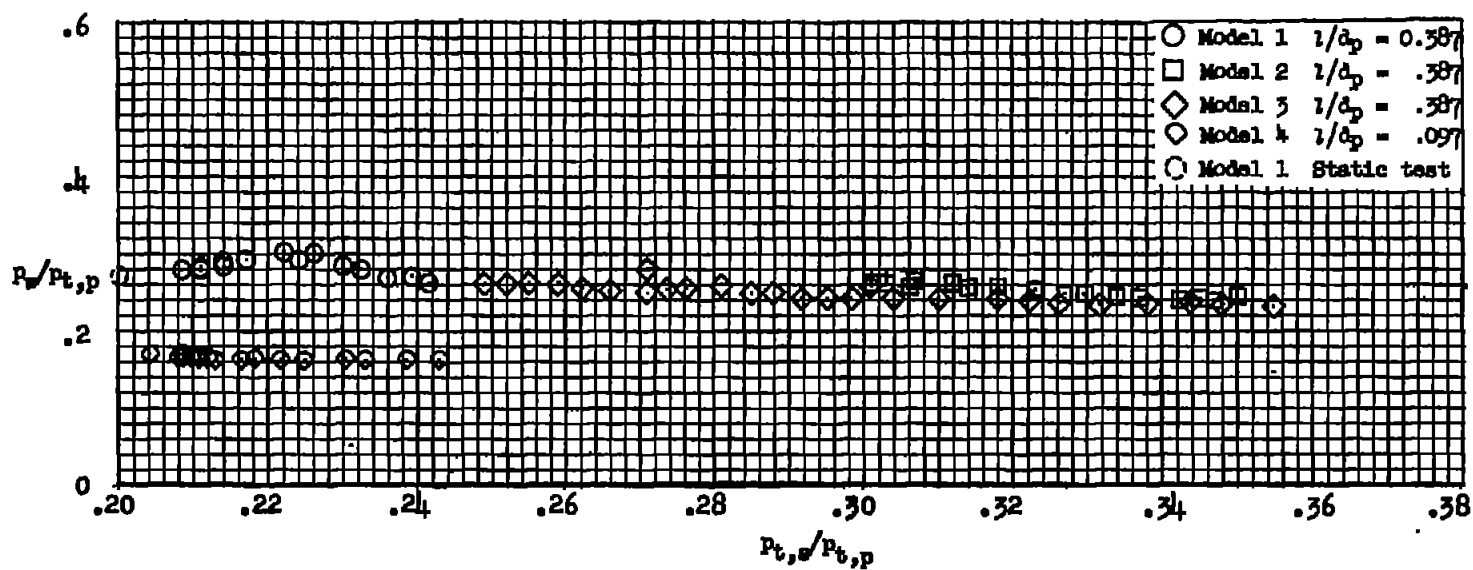(c) Model 3.
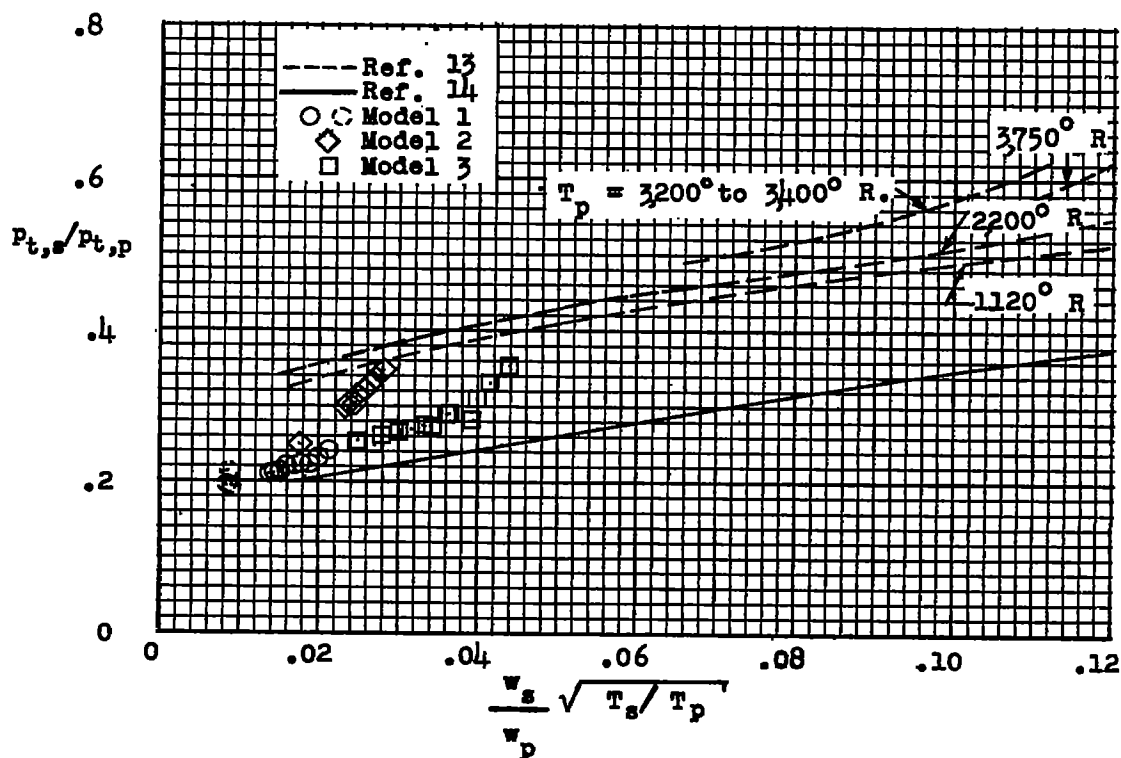

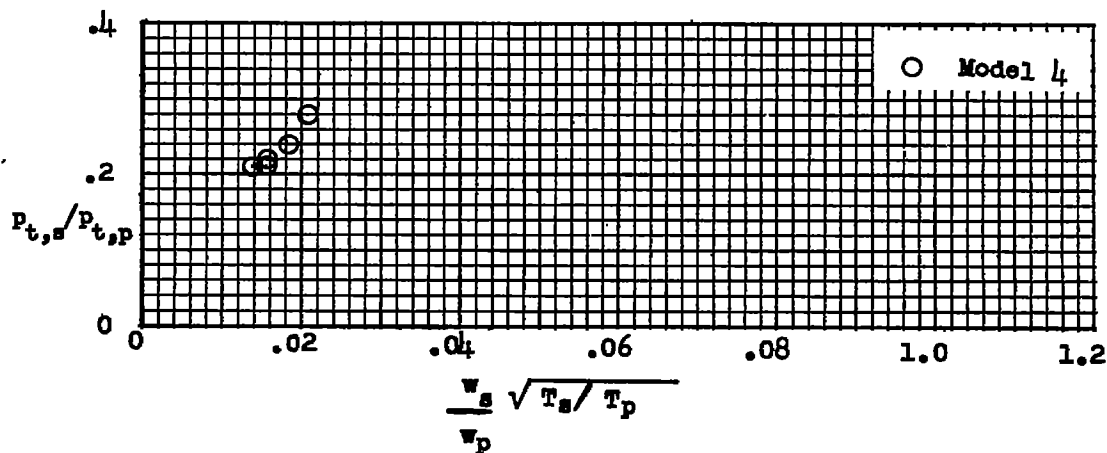(d) Model 4.

Figure 12.- Concluded.

Figure 13.- Wall-exit pressures for ejector-shroud assemblies.

(a) Spacing ratio, 0.387.

(b) Spacing ratio, 0.097.

Figure 14.- Pumping characteristics of ejector-shroud assemblies.